February 2006

NMR Structures of the Selenoproteins Sep15 and SelM Reveal Redox Activity of a New Thioredoxin-like Family

Andrew D. Ferguson
University of Texas Southwestern Medical Center, Dallas, Texas

Vyacheslav Labunskyy
University of Nebraska-Lincoln

Dmitri E. Fomenko
University of Nebraska-Lincoln, dfomenko2@unl.edu

Demet Arac
University of Texas Southwestern Medical Center, Dallas, Texas

Yogarany Chelliah
University of Texas Southwestern Medical Center, Dallas, Texas

See next page for additional authors

Published in *Journal of Biological Chemistry* 281:6 (February 10, 2006), pp. 3536-3543.
Submitted October 20, 2005; revised November 23, 2005; published online November 30, 2005, as doi:10.1074/jbc.M511386200.
This work was supported by a grant from the Welch Foundation (to J. D.) and National Institutes of Health Grant CA080946 (to V. N. G.).
The published version of this article did not contain Supplemental Tables 1 and 2 and Supplemental Figure 1, which were available online at http://www.jbc.org/; these materials are appended to the version published here.
The atomic coordinates and structure factors (code 2A2P (SelM) and 2A4H (Sep15)) have been deposited in the Protein Data Bank, Research Collaboratory for Structural Bioinformatics, Rutgers University, New Brunswick, NJ: http://www.rcsb.org/

NMR Structures of the Selenoproteins Sep15 and SelM Reveal Redox Activity of a New Thioredoxin-like Family

Andrew D. Ferguson[1,2], Vyacheslav M. Labunskyy[3], Dmitri E. Fomenko[3], Demet Araç[1,4], Yogarany Chelliah[5], Carlos A. Amezcua[1], Josep Rizo[1,4], Vadim N. Gladyshev[3], and Johann Deisenhofer[1,5,6]

[1] Department of Biochemistry, University of Texas Southwestern Medical Center, Dallas, Texas 75390; [2] Human Frontier of Science Program; [3] Department of Biochemistry, University of Nebraska–Lincoln, Lincoln, Nebraska 68588; [4] Department of Pharmacology, University of Texas Southwestern Medical Center, Dallas, Texas 75390; [5] Howard Hughes Medical Institute, University of Texas Southwestern Medical Center, Dallas, Texas 75390; [6] Corresponding author—Dept. of Biochemistry, University of Texas Southwestern Medical Center at Dallas, TX 75390. Tel.: 214-645-5941; Fax: 214-645-5939; E-mail: Johann.Deisenhofer@utsouthwestern.edu

Abstract: Selenium has significant health benefits, including potent cancer prevention activity and roles in immune function and the male reproductive system. Selenium-containing proteins, which incorporate this essential micronutrient as selenocysteine, are proposed to mediate the positive effects of dietary selenium. Presented here are the solution NMR structures of the selenoprotein SelM and an ortholog of the selenoprotein Sep15. These data reveal that Sep15 and SelM are structural homologs that establish a new thioredoxin-like protein family. The location of the active-site redox motifs within the fold together with the observed localized conformational changes after thiol-disulfide exchange and measured redox potential indicate that they have redox activity. In mammals, Sep15 expression is regulated by dietary selenium, and either decreased or increased expression of this selenoprotein alters redox homeostasis. A physiological role for Sep15 and SelM as thiol-disulfide oxidoreductases and their contribution to the quality control pathways of the endoplasmic reticulum are discussed.

Abbreviations: NOESY two-dimensional nuclear Overhauser (NOE) effect spectroscopy; HSQC, heteronuclear single quantum correlation; Bis-Tris, 2-[bis(2-hydroxyethyl)amino]-2-(hydroxymethyl)propane-1,3-diol; siRNA, small interfering RNA; UGGT, UDP-glucose:glycoprotein glucosyltransferase.

Introduction

The formation of disulfide bonds is an essential step in the structural maturation of secretory and membrane proteins. All living organisms have evolved mechanistically related pathways to catalyze the formation of disulfide bonds (1). In eukaryotes, disulfide bonds are formed primarily within the lumen of the endoplasmic reticulum. An intricate series of protein folding and quality control mechanisms localized to this organelle regulate the formation of disulfide bonds through thiol-disulfide exchange (2).

Thiol-disulfide oxidoreductases catalyze thiol-disulfide exchange between proteins with free thiols and thiol-containing small molecules or proteins with disulfide bonds. The activities of these enzymes are dependent upon active-site cysteine residues that are arranged in a C*XX*C motif or C*XX*C-derived motifs, in which one of these cysteines may be replaced by selenocysteine, serine, or threonine (3). Enzymatic activity and the direction of exchange (oxidation or reduction) depend upon redox potential, interactions with other redox proteins, and the availability of terminal electron donors and acceptors (4).

Selenium is an essential trace element that is incorporated into proteins as the 21st natural amino acid in the genetic code, selenocysteine. Selenoproteins are found throughout prokaryotic (5) and eukaryotic proteomes (6), and most have orthologs in which selenocysteine is replaced with cysteine. The identity of the active-site redox motif residues (selenocysteine or cysteine) regulates the redox potential and catalytic efficiency of these enzymes (7, 8). Recent studies provide strong evidence that dietary selenium plays an important role in cancer prevention (9–11), immune function (12), aging (13), and the male reproductive system (12, 14). Although selenoproteins appear to mediate these effects, physiological roles for most of these proteins are unknown. Two recently identified eukaryotic selenoproteins, Sep15 (15) and SelM (16), have selenocysteine-containing C*XX*C-like motifs, suggesting that they might function as redox proteins within the endoplasmic reticulum. Irrespective of this motif, these selenoproteins share no sequence similarities with known redox proteins. In an attempt to understand the physiological roles of these proteins, the solution NMR structures of fruit fly Sep15 and mouse SelM were determined. These structures identify a thioredoxin-like domain and the location of the active-site redox motif. Additional data demonstrate that these proteins undergo localized conformational changes centered on the active-site redox motif after thiol-disulfide exchange and suggest that they function as thiol-disulfide oxidoreductases that participate in the formation of disulfide bonds.

Materials And Methods

Protein Expression and Purification—Because recombinant selenoproteins are difficult to prepare in heterologous expression systems, the single selenocysteine residue (U48) in SelM from *Mus musculus* was mutated to cysteine (48U→C) to facilitate these structural studies. In contrast, Sep15 from *D. melanogaster* does not contain a selenocysteine residue and, accordingly, is a natural cysteine-containing ortholog of Sep15. The coding regions of the mouse SelM gene and the fruit fly Sep15 gene were PCR-amplified from a cDNA clone and a cDNA library (Novagen) with the following primers: 5'-TCCAGCCACCCATATGACCAACTACCGACCGGATTGGAACC-3' and 5'-GGTGGTGGTGCTCGAGGTCGTCGTGTTCTGAAGCTTCCTC-3' (residues 25-145 of SelM-48U→C including an uncleaved C-terminal hexahistidine tag (designated as SelM)) (16); 5'-AAGGGCTAGCCACCATCACCATCACCATTTGGATCAGCAGCCG-3' and 5'-AAGGCTCGAGTTAGATCCTGTTGGT-3' (residues 62-178 of Sep15 including an uncleaved N-terminal hexahistidine tag (designated as Sep15)). PCR products were digested with NdeI/XhoI (SelM) or NheI/XhoI (Sep15), ligated into pET21a (SelM) or pET19b (Sep15), and verified by DNA sequencing.

SelM and Sep15 were expressed in *Escherichia coli* BL21(DE3) cells. Cell cultures were grown at 37 °C until the A_{600} reached 0.6. Protein expression was induced by adding 0.4 mM isopropyl-β-D-thiogalacto-side, and the cells were grown for 16 h at 30 °C. After induction, bacterial cells were harvested by centrifugation at 4700 × *g* for 15 min at 4 °C, and cell pellets were re-suspended in lysis buffer (50 mM Tris (pH 8.0), 150 mM NaCl, 0.1% Triton X-100, 10 mg/liter lysozyme, 5 mg/liter DNase I, and EDTA-free Complete Protease Inhibitor Tablets (Roche Applied Science)) and lysed by sonication. Cell lysates were centrifuged at 40,000 × *g* for 30 min at 4 °C. Both proteins were purified by immobilized metal-chelate affinity, ion exchange, and gel filtration chromatography.

NMR Spectroscopy—Proteins uniformly labeled with ^{15}N or $^{13}C,^{15}N$ were produced by supplementing M9 media with 1 g/liter [^{15}N]ammonium chloride, 3 g/liter D-[^{13}C]glucose, 0.5 ml/liter 0.5% thiamine, 2 mM $MgSO_4$, 0.1 mM $CaCl_2$, 0.5 ml/liter 10 mg/ml biotin, and 100 μg/ml carbenicillin. All NMR experiments were acquired at 25 °C with Varian INOVA spectrometers operating at proton frequencies of 500 and 600 MHz using 1 mM protein samples dissolved in 50 mM sodium phosphate (pH 6.0) and 50 mM NaCl. NMR data were processed with NMRPipe (17) and analyzed with NMRView (18). Backbone and aliphatic side chain chemical shift assignments were obtained from standard triple resonance experiments: HNCO, HNCACB, CBCA(CO)NH, HNHA, C(CO)NH-two-dimensional total correlation spectroscopy (TOCSY), H(CCO)NH-TOCSY, and HCCH-TOCSY. Aromatic side chain chemical shifts were assigned with two-dimensional double quantum filtered correlation spectroscopy and NOESY[3] (τ_m = 100 ms) experiments using ^{15}N-labeled protein samples in 99.9% D_2O. Stereospecific chemical shift assignments for valine and leucine methyl groups were obtained with two constant time ^1H, ^{13}C HSQC experiments (28- and 43-ms delay) using 10% ^{13}C uniformly labeled samples (19). Residual dipolar couplings were extracted from in-phase anti-phase experiments using ^{15}N-labeled samples aligned in 5% polyacrylamide stretched gels (20).

Distance restraints were obtained from three-dimensional ^{15}N-edited NOESY (τ_m = 100 ms) and ^{13}C-edited NOESY (τ_m = 100 ms) spectra recorded from ^{15}N- and $^{13}C,^{15}N$-labeled proteins. Restraints for the dihedral backbone angles (φ,ψ) were derived from an analysis of $^{13}C\alpha$, $^{13}C\beta$, ^{13}CO, and ^{15}N chemical shifts using TALOS (21). Error bounds for these restraints were set to twice the S.D. of the predictions with a minimum bound of ±30°. Hydrogen bond restraints were established for those amide protons protected from D_2O exchange in $^1H,^{15}N$ HSQC experiments.

Structure calculations were performed with ARIA (22). ARIA runs were initiated using a set of NOEs manually assigned from ^{15}N-edited NOESY spectra. NOEs from ^{13}C-edited NOESY spectra were introduced into the calculation once an initial ensemble of low energy structures was obtained. MOLMOL (23) was used to assign carbonyl partners for amide protons that were protected from D_2O exchange. Hydrogen bond restraints were set to 1.3 Å < d_{NH-O} < 2.5 Å and 2.3 Å < d_{N-O} < 3.5 Å, respectively. Protein alignment tensors calculated with PALES (24) were used for structural refinement against residual dipolar coupling data. Structural coordinates have been deposited in the Protein Data Bank and have been assigned the accession codes 2A2P (SelM) and 2A4H (Sep15).

Redox Potential—Analysis of the equilibrium redox potential of fruit fly Sep15 (residues 62-178) was performed as previously described (25). Sep15, contained in 100 mM sodium phosphate (pH 7.0), 1 mM EDTA, and various concentrations of reduced and oxidized glutathione, was incubated at room temperature for 12 h. Protein samples were precipitated with cold 15% trichloroacetic acid for 15 min, centrifuged at 15,000 × *g* for 10 min, washed with cold acetone, and dried. Samples were re-suspended in buffer (100 mM sodium phosphate (pH 7.0), 1 mM EDTA and 1% SDS) and alkylated with 15 mM 4-acetamido-4'-maleimidylstilbene-2,2'-disulfonic acid (Molecular Probes) for 2 h at 37°C. Alkylated samples were resolved by SDS-PAGE using NuPAGE Bis-Tris gels under reducing conditions followed by Western blotting using Sep15-specific antibodies. The redox potential was calculated using the Nernst equation as previously described (26).

RNA Interference, Overexpression, and Oxidative Stress—Four siRNA expression cassettes (designated S1-S4) targeted against different regions of mouse Sep15 mRNA were generated using the Silencer Express Kit (Ambion) according to the manufacturer's instructions. The following primers were used: S1, 5'-TGCCTACACAAAGCAAGAGCTGCAGAGCAAGCGGTGTTTCGTCCTTTCCACAAG-3' and 5'-CGGCGAAGCTTTTTCCAAAAAACTTGCTCTGCAGCTCTTGCCTACACAAAGCAA-3'; S2, 5'-ATCCTACACAAAGATGGCTCCTGCATACAGCCGGTGTTTCGTCCTTTCCACAAG-3' and 5'-CGGCGAAGCTTTTTCCAAAAAAGCTGTATGCAGGAGCCATCCTACACAAAGATG-3'; S3, 5'-GACCTACACAAAGTCTGAGCCTCGAACATACCGGTGTTTCGTCCTTTCCACAAG-3' and 5'-CGGCGAAGCTTTTTCCAAAAAAGTATGTTCGAGGCTCAGACCTACACAAAGTCT-3'; S4, 5'-AGTCTACACAAAACTTCTCGCTCAGGAACTCCGGTGTTTCGTCCTTTCCACAAG-3' and 5'-CGGCGAAGCTTTTTCCAAAAAAGAGTTCCTGAGCGAGAAGTCTACACAAAACTT-3'. PCR products were digested with EcoRI/HindIII, ligated into the pSEC-hygro vector, and verified by DNA sequencing.

Mouse fibroblast NIH-3T3 cells were grown in Dulbecco's modified Eagle's medium supplemented with 10% fetal calf serum to ~80% confluence. Transfections were performed using Lipofectamine and PLUS reagent (Invitrogen) according to the manufacturer's instructions. For each 60-mm plate, 2 μg of DNA, 8 μl of PLUS reagent, and 12 μl of Lipofectamine were used. Twenty-four hours after transfection cells stably expressing Sep15-specific siRNA were isolated by resistance to hygromycin B. Down-regulation of Sep15 mRNA expression was confirmed by Northern blotting using a Sep15-specific probe. To ensure equal loading of RNA, Northern blots were stripped and re-probed using a glycelaldehyde-3-phosphate dehydrogenase-specific probe. Protein expression was assayed by Western blotting using Sep15-specific antibodies. Cells stably transfected with S4-siRNA were used to assess the sensitivity to oxidative stress.

The coding region of the mouse Sep15 gene was PCR-amplified from a cDNA clone with the following primers: 5'-CATTAGTATCTAATCTCGAGGGCAGACCGCAGGGAT-3' and 5'-CTCGAGGGATACTCTAGAGCG-3'. The PCR product was digested with XhoI/NotI and ligated into the pCI-neo vector (designated Sep15/pCI-neo). Mutagenesis of the mouse Sep15 gene was carried out using the QuikChange site-directed mutagenesis kit (Stratagene). The following mutagenic primers were used to replace the selenocysteine residue: 5'-CTTGAAGTCTGCGGATGTAAATTGGGGAGGTTCC-3' and 5'-GGAACCTCCCCAATTTACATCCGCAGACTTCAAG-3'. Expected sequence changes were verified by DNA sequencing (designated Sep15-U93C/pCI-neo). NIH-3T3 cells were transfected with these plasmids as described above. Stable transfectants were isolated by resistance to G418.

The sensitivity of NIH-3T3 cells to oxidative stress was analyzed with the CellTiter 96 AQ_{ueous} One Solution Cell Proliferation Assay (Promega). 5×10^3 of cells were seeded into each well of 96-well plates and grown overnight in Dulbecco's modified Eagle's medium supplemented with 10% fetal calf serum. Cells were washed twice with phosphate-buffered saline and incubated in serum/phenol red-free medium containing *tert*-butyl hydroperoxide and cumyl hydroperoxide for 1 h at 37 °C in a humidified 5% CO_2 incubator. 20 μl of CellTiter 96 AQ_{ueous} One Solution reagent was added to each well and incubated for an additional four hours. The A_{490} was recorded using an ELx808 Ultra microplate reader (Bio-Tek Instruments). Cell viability is expressed as the percentage of untreated controls.

Expression Pattern Analysis—Four-month-old male BALB/c mice were maintained on a Torula yeast diet (Harland Teklad) supplemented with 0, 0.1, or 0.4 ppm selenium in the form of Na_2SeO_3 for 1 month. Tissues were homogenized in CelLytic-M lysis buffer (Sigma) containing EDTA-free Complete Protease Inhibitor Tablets by sonication and centrifuged at 15,000 × *g* for 20 min. The expression patterns of Sep15, glutathione peroxidase 1, and thioredoxin reductase 3 were analyzed by Western blotting using antibodies against these proteins.

Results

Structure Determination—Although SelM and Sep15 are distant sequence homologs, they do share regions of significant sequence identity. Multiple sequence alignments were used to define the boundaries of a putative homologous domain that is shared between these proteins. Residues 1-23 of mouse SelM and residues 1-16 of fruit fly Sep15 form signal sequences that are cleaved during protein maturation. The chemical shift dispersion of the $^1H,^{15}N$ HSQC spectra of full-length SelM (residues 24-145) and full-length Sep15 (residues 17-178) revealed the presence of poorly ordered regions in Sep15. By comparing the $^1H,^{15}N$ HSQC spectra of Sep15 with different construct boundaries, we determined that the N terminus of Sep15 (residues 17-61) was disordered. The high resolution solution NMR structures of mouse SelM-48U→C (residues 25-145) and the homologous region of fruit fly Sep15 (residues 62-178) were determined under oxidizing conditions by standard double and triple resonance experiments using protein samples uniformly labeled with ^{15}N or $^{13}C,^{15}N$ (Table 1). A combination of proton-proton distances, dihedral angles, hydrogen bonds, and residual dipolar couplings were used in the structural calculations (Figure 1*A*).

Overall Description of the Structure—SelM and Sep15 contain a central α/β domain (22% sequence identity) that is composed of three α-helices (α1- α3) and a mixed parallel/anti-parallel four-stranded β-sheet (β1- β4) (Figure 1, *A* and *B*). Conserved residues primarily form the internal core of this domain and delineate each of the secondary structural elements (Figure 2). Structure-based multiple sequence alignments illustrate that SelM has a short N-terminal extension that precedes strand β1 and a flexible C-terminal extension after helix α3. In contrast, Sep15 has an elongated cysteine-rich N-terminal extension before strand β1 and a shorter C-terminal extension after helix α3 that does not adopt a regular secondary structure. The sequence of the N-terminal extension of Sep15 is highly conserved among Sep15 homologs and is conversely absent in sequence homologs of SelM (Figure 2).

Comparing the structures of the redox domains of SelM and Sep15 with DaliLite (27) shows an overall root mean square deviation of 1.9 Å when comparing the Cα positions of residues 38-112 of SelM and residues 73-147 of Sep15 (Supplemental Figure 1*A*). A search of the DALI data base of protein structures (28) identified members of the thioredoxin superfamily as the closest structural relatives for these proteins. The highest similarities were obtained for subunit B8 from human NADH ubiquinone oxidoreductase complex I (29), *Anabaena* thioredoxin 2 (30), and human thioredoxin (31) (Supplemental Tables 1 and 2).

Proteins involved in the regulation of intracellular redox homeostasis and redox-sensitive protein folding pathways often contain thioredoxin-like domains. The classical thioredoxin fold is described as a three-layer α/β/α sandwich composed of a mixed five-stranded β-sheet and two pairs of α-helices that are found on either side of the β-sheet (32) (Supplemental Figure 1*B*). A recent comprehensive structural classification of the thioredoxin-like fold (33) describes it as a two-layer α/β sandwich composed of a mixed four-stranded β-sheet and a pair of α-helices that are packed against one side of

TABLE 1. Structural statistics for the twenty lowest energy SelM and Sep 15 structures

List of restraints	SelM	Sep15
NOE distance restraints	2761	1904
Unambiguous	2665	1879
Ambiguous	96	25
Hydrogen bond restraints	47	36
Dihedral angle (ϕ,ψ) restraints from TALOS	72	51
$^1H,^{15}N$ residual dipolar couplings	40	19
Structural analysis		
Average number of NOE violations >0.5 Å	0.35 ± 0.57	0.15 ± 0.36
Average number of dihedral violations >5°	2.9 ± 1.10	0.24 ± 0.43
Ramachandran plot[a]		
Most favored	80.4%	80.8%
Additionally allowed	19.6%	19.2%
Generously allowed	0%	0%
Disallowed	0%	0%
Deviations from idealized geometry[b]		
Bond, Å	0.003 ± 0.0002	0.003 ± 0.0001
Angles, °	0.488 ± 0.010	0.414 ± 0.013
Impropers, °	0.442 ± 0.049	0.384 ± 0.024
Deviations from experimental restraints[b]		
Dihedral angles, °	1.852 ± 0.119	0.722 ± 0.136
Residual dipolar couplings, Hz	0.330 ± 0.048	0.363 ± 0.201
Deviations from average structure[a]		
Backbone, Å	0.28 ± 0.08	0.45 ± 0.11
Heavy atoms, Å	0.80 ± 0.20	0.83 ± 0.20

[a] Calculated with PROCHECK-NMR (55) using residues 36–44, 54–73, 80–85, 89–97, and 100–116 (SelM) and 71–80, 89–95, 98–119, 127–132, and 139–149 (Sep15).
[b] Calculated with ARIA.

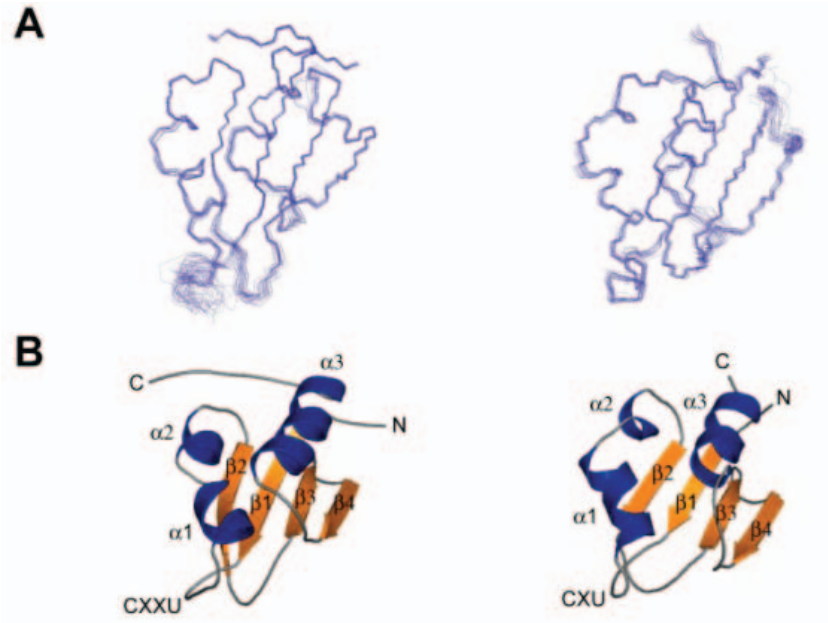

FIGURE 1. **Solution NMR structures of SelM and Sep15.** *A*, backbone superposition of the 20 lowest energy structures of SelM (*left panel*) and Sep15 (*right panel*). *B*, ribbon representation of the SelM (*left panel*) and Sep15 (*right panel*) structures that are closest to the mean with α-helices colored *blue* (α1-α3), β-strands colored *orange* (β1- β4), and coils colored *gray*. The locations of the redox-active motifs for SelM (*CXXU*) and Sep15 (*CXU*) are indicated. Residues 25-34 and residues 121-145 (including an uncleaved C-terminal hexahistidine tag) of SelM are not shown because these regions are flexible. Residues 62-70 (including an uncleaved N-terminal hexahistidine tag) and residues 150-178 of Sep15 are not shown because these regions are also flexible. This figure was prepared with MOLMOL and PyMOL (52).

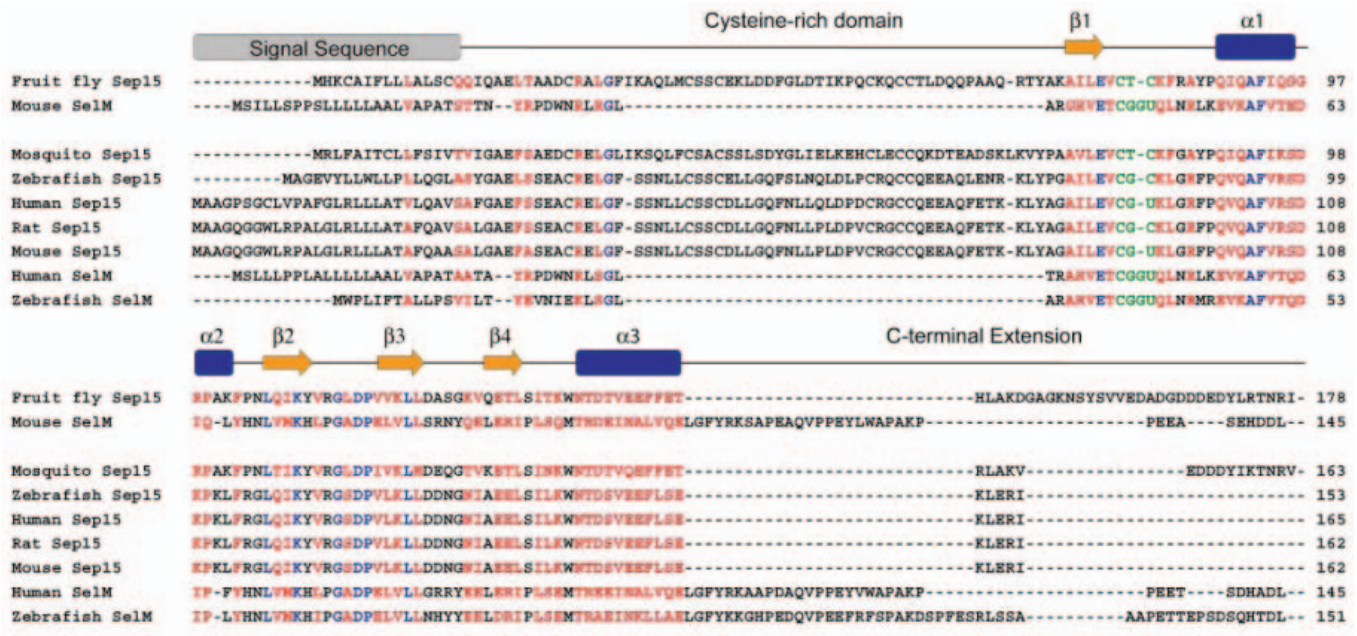

FIGURE 2. **Structure-based multiple sequence alignment of SelM and Sep15 homologs.** Assigned secondary structure elements for SelM and Sep15 are indicated *above* each sequence with α-helices colored *blue* and β-strands colored *orange*. Strictly conserved residues are shown in *blue*, and moderately conserved residues are shown in *red*. The active-site redox motif, including the selenocysteine residue (*U*), is colored *green* and is located between the C terminus of strand β1 and the N terminus of helix α1. The following accession numbers were used to generate this alignment: human SelM (27805722); mouse SelM (23956246); zebrafish SelM (29648551); human Sep15 (6094261); mouse Sep15 (20140242); zebrafish Sep15 (68053306); rat Sep15 (20139870); mosquito (18389881); fruit fly Sep15 (24666045). This alignment was produced with 3D-COFFEE (53).

the β-sheet. Although SelM and Sep15 share structural similarities with other proteins containing thioredoxin-like domains, these NMR structures represent the most basic thioredoxin-like fold, containing only the core secondary structure elements as defined by Qi and Grishin (33).

Sequence and structural motifs can be used to assign which family within the thioredoxin superfamily putative thiol-disulfide oxidoreductases may belong (33); however, such comparisons do not provide direct evidence of biological function. Using the structural consensus of thioredoxin homologs and circular permutations of this fold (33), all structurally defined proteins containing thioredoxin-like domains have been grouped into eleven evolutionary families based on sequence, structural, and functional evidence. A manual structure-based alignment of SelM and Sep15 demonstrates that they are clearly members of the thioredoxin family; however, they do form a distinct subfamily within that family. As observed with other proteins with thioredoxin-like domains, the unusual active-site redox motifs of SelM (CGGU) and Sep15 (CGU) are located between the C terminus of strand β1 and the N terminus of helix α1 (Figure 1*B*). The fold and location of these redox motifs suggest redox activity for Sep15 and

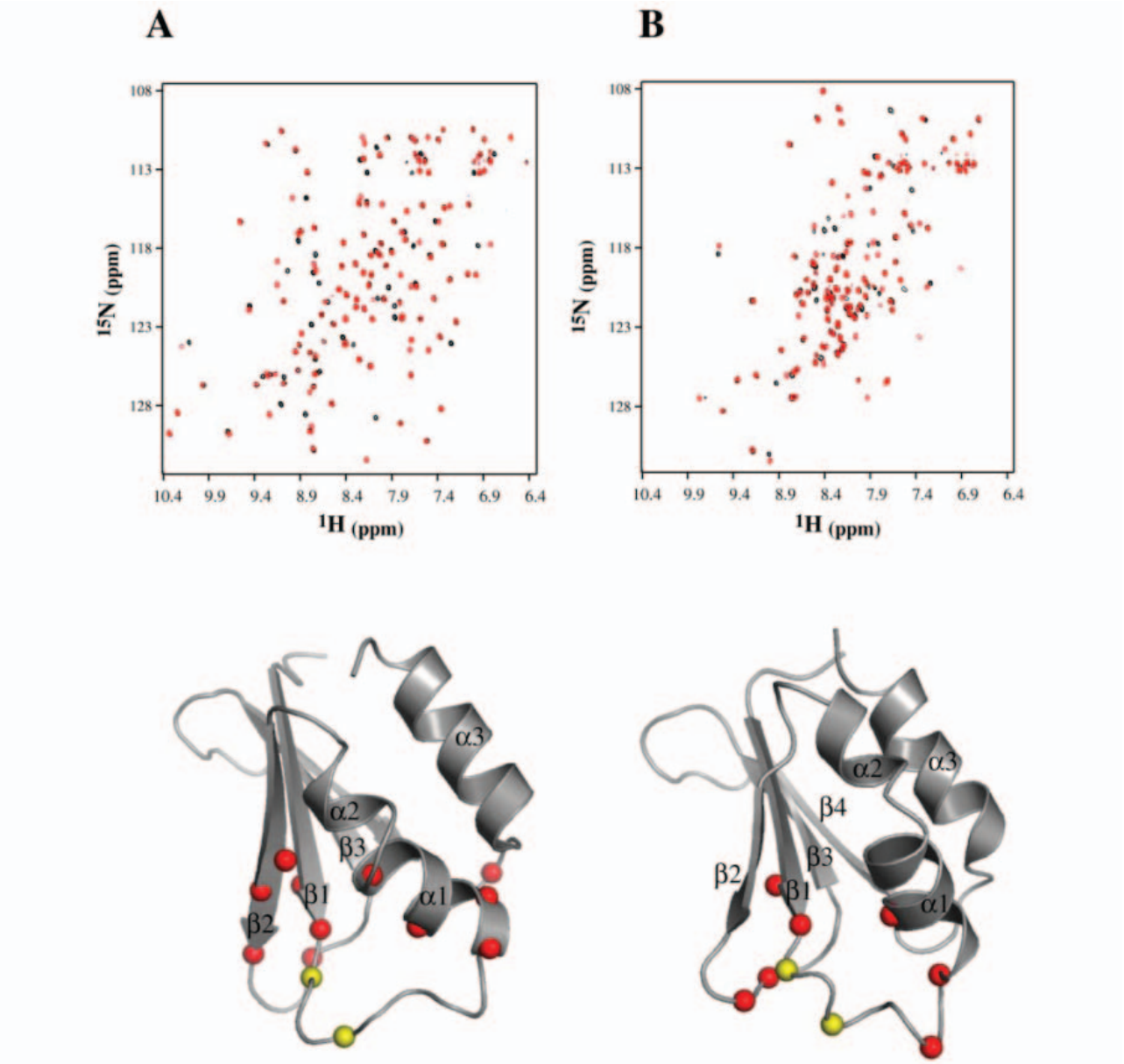

FIGURE 3. **Identification of residues effected by thiol-disulfide exchange in SelM and Sep15.** *A*, $^{1}H,^{15}N$ HSQC spectra of SelM. *B*, Sep15 without (*black*) and with (*red*) 2 mM dithiothreitol (*top panel*). Amide protons of those residues experiencing minimum chemical shift changes (54) ($\Delta\delta = ([\Delta\delta^{1}H]^2 + 0.1 \times [\Delta\delta^{15}N]^2)^{1/2}$) of one S.D. above the mean (SelM $\Delta\delta > 0.11$ ppm and Sep15 $\Delta\delta > 0.12$ ppm) are shown as *red spheres (bottom panel*). *Yellow spheres* indicate the location of the cysteine and selenocysteine residues that compose the active-site redox motif.

SelM. However, the consensus sequences of the active-site motifs of thioredoxins (CGPC), protein disulfide isomerases (CGHC) and disulfide oxidases (CPHC) are different from those of SelM (CGGC) and Sep15 (CG/TC) (4, 33). Many structurally defined members of the thioredoxin superfamily have a conserved *cis*-proline residue placed near the N terminus of strand β3 (33). Although SelM and Sep15 do indeed have prolines located at these positions, they are in the *trans*-conformation. However, a charge pair that is involved in the proton transfer reaction in thioredoxin (4, 34) and protein disulfide isomerase (4, 35) is not found in SelM and Sep15. Nevertheless, given the similarities to other characterized thiol-disulfide oxidoreductases (32, 33), the surface accessibility and unusual composition of the active-site redox motif, the presence of residues known to influence the activity of other redox proteins suggests that SelM and Sep15 are thiol-disulfide oxidoreductases that are capable of forming reversible mixed selenenylsulfide bonds during the catalytic cycle of oxidation and reduction.

Structural Effect of Active-site Disulfide Bond Reduction—The chemical shift dispersion of the $^{1}H,^{15}N$ HSQC spectra for the oxidized and reduced forms of SelM (Figure 3*A*) and Sep15 (Figure 3*B*) indicates that they remain folded in both oxidation states. Comparing the oxidized and reduced ^{1}H, ^{15}N HSQC spectra demonstrates that most of the backbone amide resonances are unchanged by the reduction of the active-site disulfide bond and that thiol-disulfide exchange is not accompanied by a large conformational change. However, significant changes in backbone amide resonances were observed for some residues. These differences are consistent with a localized structural rearrangement centered on the active-site redox motifs of SelM (Figure 3*A*) and Sep15 (Figure 3*B*). Comparison of the oxidized and reduced forms of thioredoxin also shows similar changes surrounding the active-site redox motif (36).

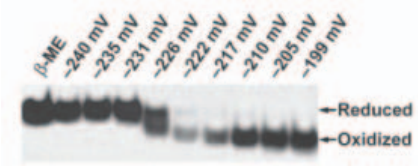

FIGURE 4. **Determination of the equilibrium redox potential of Sep15.** 10-μg aliquots of Sep15 (residues 62-178) were equilibrated in buffers containing defined ratios of reduced-to-oxidized glutathione (-240 mV (10 mM GSH/0.1 mM GSSG), -235 mV (10 mM GSH/0.15 mM GSSG), -231 mV (10 mM GSH/0.2 mM GSSG), -226 mV (10 mM GSH/0.3 mM GSSG), -222 mV (10 mM GSH/0.4 mM GSSG), -217 mV (10 mM GSH/0.6 mM GSSG), -210 mV (10 mM GSH/1 mM GSSG), -205 mV (10 mM GSH/1.5 mM GSSG), and -199 mV (10 mM GSH/2.5 mM GSSG)]) or treated with β-mercaptoethanol (β-*ME*) before the addition of the thiol-alkylating agent 4-acetamido-4'-maleimidylstilbene-2,2'-disulfonic acid as a control. Alkylation of reduced cysteine residues leads to an increase in molecular mass and altered electrophoretic mobility. These samples were resolved by reducing SDS-PAGE and analyzed by Western blotting using Sep15-specific antibodies. Using the Nernst equation (26), the equilibrium redox potential of Sep15 was calculated to be -225 mV.

Redox Potential—As thiol-disulfide oxidoreductases, SelM and Sep15 are potentially involved in the formation, reduction, or isomerization of disulfide bonds. The propensity of these proteins to donate or accept electrons can be expressed as an equilibrium redox potential. Biological roles for thiol-disulfide oxidoreductases can be inferred by comparing relative redox potentials. Because preparation of selenoproteins in large quantities is difficult and a selenocysteine-free ortholog of SelM could not be identified in higher eukaryotes, its equilibrium redox potential was not determined. However, using the Nernst equation, the redox potential of fruit fly Sep15 (residues 62-178) was calculated and found to be –225 mV (Figure 4). The redox potentials of selenocysteine-containing Sep15 proteins might differ from that of the cysteine-containing fruit fly Sep15 but should be close to it to maintain the function. The calculated redox potential of fruit fly Sep15 is higher than that of the strong disulfide reductant thioredoxin (-270 mV (37, 38)) and is lower than that of the disulfide oxidase DsbA (-122 mV (39, 40)). The redox potential of Sep15 is between that of thioredoxin and protein disulfide isomerase (-175 mV (37)), suggesting that Sep15 may plausibly catalyze the reduction and/or isomerization of disulfide bonds in secreted proteins (4). However, the biological activities of redox proteins within the endoplasmic reticulum lumen are influenced by protein-protein interactions with other resident redox proteins, thiol-containing molecules, such as glutathione, and molecular oxygen (39). Thus, there may be discrepancies between the *in vitro* and *in vivo* redox potentials of Sep15.

Regulation of Sep15 Expression and Oxidative Stress—RNA interference was used to suppress Sep15 gene expression. NIH-3T3 cells were transfected with constructs expressing siRNA targeted against different regions of mouse Sep15 mRNA (Figure 5*A*, *S1-S4*). Northern blots demonstrate that the expression of Sep15 mRNA was reduced to less than 10% that of wild-type levels for two of the four siRNAs tested (Figure 5*A*). Western blots confirmed the decrease in Sep15 protein expression for S4-siRNA (Figure 5*B*). Depletion of Sep15 mRNA by RNA interference increased the viability of these cells to treatment with *tert*-butyl hydroperoxide and cumyl hydroperoxide (Figure 5, *C* and *D*). To determine whether overexpression of Sep15 might protect cells against oxidative stress, stable cell lines that overexpress wild-type mouse Sep15 or Sep15-U93C were developed (Figure 6*A*). Cell viability assays indicate that overexpression of Sep15 or Sep15-U93C also results in increased susceptibility to oxidative stress (Figure 6, *B* and *C*). These data reveal that altered Sep15 expression disrupts the redox homeostasis of the endoplasmic reticulum.

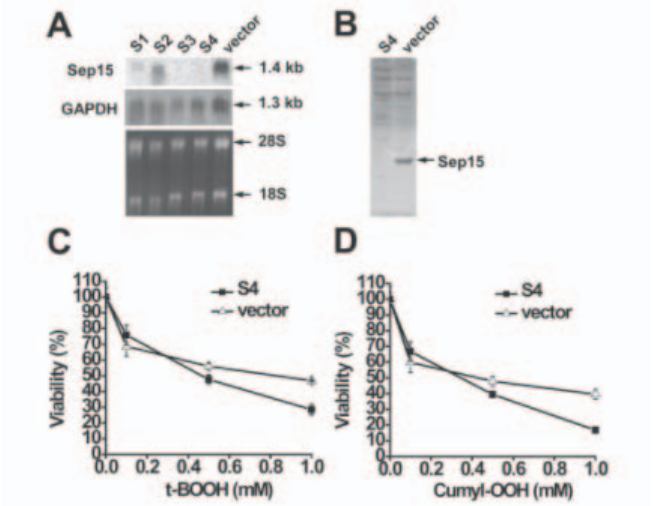

FIGURE 5. **Viability of Sep15 RNAi knockdown cells to oxidative stress.** *A*, Northern blot of Sep15 mRNA levels in NIH-3T3 cells stably transfected with constructs expressing siRNA targeted against different regions of Sep15 mRNA (S1-S4). Expression of Sep15 mRNA is down-regulated by S1, S3, and S4 (*top panel*). Glycelaldehyde-3-phosphate dehydrogenase (*GAPDH*) and ribosomal RNA (28 S and 18 S) controls are shown in the *middle* and *lower panels*, respectively. *kb*, kilobases. *B*, Western blot of Sep15 protein expression. *C*, viability of cells to *tert*-butyl hydroperoxide (*t-BOOH*) treatment. *D*, viability of cells to cumyl hydroperoxide treatment. Results are presented as the mean ± S.D. of four replicate experiments.

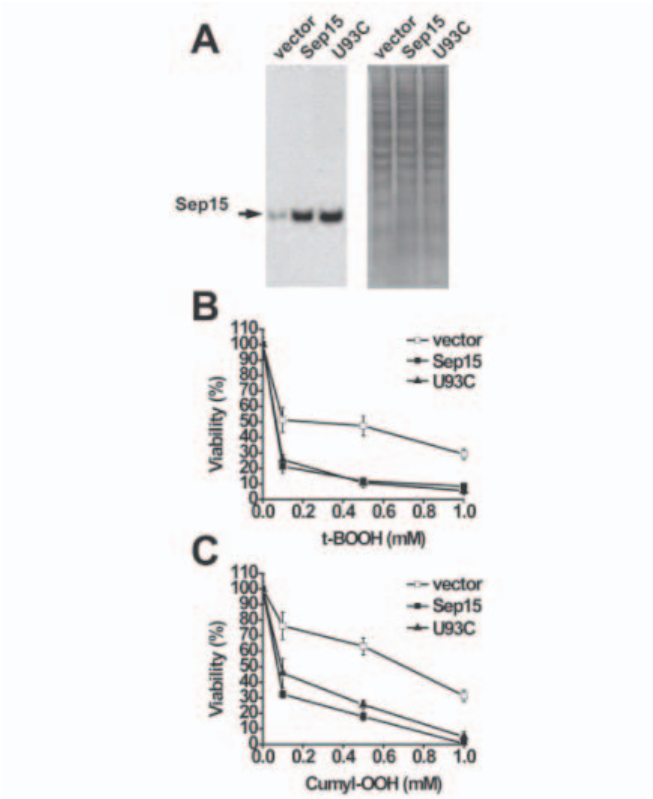

FIGURE 6. **Viability of cells overexpressing Sep15 or Sep15-U93C to oxidative stress.** *A*, Western blot of Sep15 protein expression (*left panel*) and naphthol blue-black staining of the control gel (*right panel*). *B*, viability of cells overexpressing Sep15 or Sep15-U93C to *tert*-butyl hydroperoxide (*t-BOOH*) treatment. *C*, viability of cells overexpressing Sep15 or Sep15-U93C to cumyl hydroperoxide treatment. Results are presented as the mean ± S.D. of four replicate experiments.

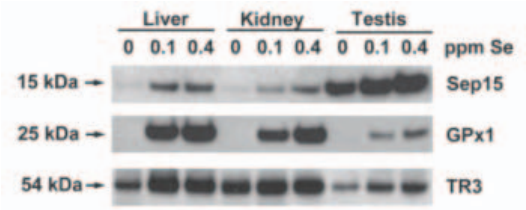

FIGURE 7. **Regulation of Sep15 expression by dietary selenium.** Tissue extracts from mice maintained on diets containing 0, 0.1, or 0.4 ppm dietary selenium were resolved by SDS-PAGE and analyzed by Western blotting with antibodies specific for Sep15 (*top panel*), glutathione peroxidase 1 (*GPx1*) (*middle panel*), and thioredoxin reductase 3 (*TR3*) (*bottom panel*).

Regulation of Sep15 Expression by Dietary Selenium—The differential expression of Sep15 in response to selenium availability was assayed. Mice maintained on a Torula yeast diet supplemented with 0, 0.1, or 0.4 ppm selenium was sacrificed after 1 month of dietary selenium supplementation. Western blotting was used to determine the expression patterns of Sep15, glutathione peroxidase 1 and thioredoxin reductase 3 (Figure 7). Sep15 expression was reduced in the liver and kidneys of mice maintained on a selenium-deficient diet as compared with those maintained with 0.1 and 0.4 ppm selenium. In contrast, Sep15 expression in the testes was less responsive to selenium deficiency. We were unable to detect glutathione peroxidase 1 expression under selenium-deficient conditions in these tissues. As observed with Sep15, the expression pattern of thioredoxin reductase 3 was less responsive to the availability of selenium. These data are consistent with previous studies showing that the expression patterns of selenoproteins localized to the liver and kidneys are highly responsive to the availability of selenium and that the testes retain the majority of selenium under selenium-deficient conditions (41, 42). The underlying mechanism for this asymmetric distribution of selenium is unknown.

Discussion

Thiol-disulfide oxidoreductases (including thioredoxins, protein disulfide isomerases, and disulfide oxidases) catalyze the correct formation of disulfide bonds. Although a growing number of eukaryotic protein disulfide isomerases have been identified in the endoplasmic reticulum (4), biological activities for most of these proteins remain unknown. Protein disulfide isomerases typically consist of two catalytic thioredoxin-like domains (a and a') that each contain an active-site redox motif which are separated by two non-catalytic thioredoxin-like domains (b and b'). However, some protein disulfide isomerases, such as ERp18 (43) and ERp44 (44), only possess a single catalytic a-domain. By analogy to human protein disulfide isomerase, SelM and Sep15 are composed of one catalytic a-domain that assumes a thioredoxin-like fold composed of a mixed four-stranded β-sheet and three interspersed α-helices. The secondary structure elements that form this thioredoxin-like domain appear to be highly conserved among SelM and Sep15 homologs. Although members of the thioredoxin superfamily were identified as the closest structural relatives for SelM and Sep15, sequence and structural comparisons demonstrate that they form a distinct evolutionary family. As observed in thioredoxin (32, 36) and the a-domain of human protein disulfide isomerase (45), the active-site redox motifs of SelM and Sep15 are located between the C terminus of strand β1 and the N terminus of helix α1. In contrast to thioredoxin, both active-site redox residues (cysteine or selenocysteine) are surface-accessible, as found in the a-domain of protein disulfide isomerase. The unusual selenocysteine-containing redox motifs of SelM and Sep15 are capable of forming reversible mixed selenenylsulfide bonds during the catalytic cycle of oxidation and reduction. Reduction of the active-site disulfide (or selenenylsulfide) bond results in localized conformational changes that are centered on the redox motif. The calculated redox potential of fruit fly Sep15 (–225 mV) lies in between that of thioredoxin and protein disulfide isomerase, suggesting that Sep15 may catalyze the reduction and/or isomerization of disulfide bonds by functioning as a weak reductant or protein disulfide isomerase. Although the introduction of a selenocysteine residue into the active-site redox motif would lower the equilibrium redox potential, there may be compensatory sequence changes that may equalize the redox potentials of cysteine and selenocysteine-containing orthologs.

The non-catalytic b'-domain of human protein disulfide isomerase functions as the primary binding site for peptide and protein substrates. The highly flexible C-terminal extensions of SelM (residues 121-145) and Sep15 (residues 150-178) may perform an analogous role and assume a defined conformation after the binding of protein substrates or other redox proteins. The N-terminal extension of SelM (residues 25-34) is relatively short, whereas the equivalent region of Sep15 (residues 17-61) forms a distinct cysteine-rich domain. A short linker (residues 62-70) connects the N- and C-terminal domains of Sep15. The cysteine-rich domain of Sep15 has an established function; it mediates the formation of a high affinity 1:1 complex (apparent K_D of 20 nM) between Sep15 and the folding sensor of the calnexin cycle-UDP-glucose:glycoprotein glucosyltransferase (UGGT) (46, 47). SelM and its homologs do not contain an equivalent region and, accordingly, do not form complexes with UGGT (46).

The calnexin cycle is an essential quality control pathway localized to the endoplasmic reticulum that assists in the folding of *N*-linked glycoproteins. Selenoproteins have not previously been shown to be involved in the quality control pathways of the endoplasmic reticulum. However, the observation that Sep15 co-purifies with UGGT indicates that this selenoprotein may be indirectly involved in the calnexin cycle by likely functioning as a protein disulfide isomerase co-factor that assists UGGT in assessing the structural fidelity of misfolded glycoproteins. Alternatively, UGGT may have a role of a primary binding site for Sep15 substrates, analogous to the non-catalytic b'-domain of human protein disulfide isomerase.

In contrast to protein disulfide isomerase and its broad substrate specificity, SelM and Sep15 may service a restricted group of protein substrates as demonstrated for protein disulfide isomerase ERp57 (a member of the calnexin cycle), which functions exclusively as an isomerase for partially folded glycoproteins that are bound to the chaperones calnexin and calreticulin (48–50). Large multiprotein complexes that are composed of various chaperones form networks within the lumen of the endoplasmic reticulum (51). These preformed complexes concentrate multiple chaperones and other folding enzymes upon newly synthesized proteins and prevent partially folded proteins from prematurely progressing through the secretory pathway. The association of Sep15 with UGGT directly links this selenoprotein to these networks. The biochemical and structural data presented here suggest that unusual active-site redox motif of Sep15 may participate in the reduction or isomerization of disulfide bonds of glycoprotein substrates of UGGT.

Collectively, the identification of a thioredoxin-like domain and the presence of a surface-accessible active-site redox motif, sequence, and structural similarities to other characterized thiol-disulfide oxidoreductases and the determination of the redox potential of Sep15 suggest that SelM and Sep15 are thiol-disulfide isomerases that are involved in disulfide bond formation in the endoplasmic reticulum.

Acknowledgments — *We thank P. A. J. Erbel, K. H. Gardner, N. V. Grishin, Y. Qi, and R. I. Sadreyev for technical assistance and helpful discussions.*

References

1. Sevier, C. S., and Kaiser, C. A. (2002) *Nat. Rev. Mol. Cell Biol.* **3,** 836-847
2. Ellgaard, L., and Helenius, A. (2003) *Nat. Rev. Mol. Cell Biol.* **4,** 181-191
3. Fomenko, D. E., and Gladyshev, V. N. (2003) *Biochemistry* **42,** 11214-11225
4. Ellgaard, L., and Ruddock, L. W. (2005) *EMBO Rep.* **6,** 28-32
5. Kryukov, G. V., and Gladyshev, V. N. (2004) *EMBO Rep.* **5,** 538-543
6. Kryukov, G. V., Castellano, S., Novoselov, S. V., Lobanov, A. V., Zehtab, O., Guigo, R., and Gladyshev, V. N. (2003) *Science* **300,** 1439-1443
7. Stadtman, T. C. (1996) *Annu. Rev. Biochem.* **65,** 83-100
8. Gromer, S., Johansson, L., Bauer, H., Arscott, L. D., Rauch, S., Ballou, D. P., Williams, C. H., Jr., Schirmer, R. H., and Arner, E. S. (2003) *Proc. Natl. Acad. Sci. U. S. A.* **100,** 12618-12623
9. Clark, L. C., Combs, G. F., Jr., Turnbull, B. W., Slate, E. H., Chalker, D. K., Chow, J., Davis, L. S., Glover, R. A., Graham, G. F., Gross, E. G., Krongrad, A., Lesher, J. L., Jr., Park, H. K., Sanders, B. B., Jr., Smith, C. L., and Taylor, J. R. (1996) *J. Am. Med. Assoc.* **276,** 1957-1963
10. Zhang, Z., Kimura, M., and Itokawa, Y. (1997) *Biol. Trace Elem. Res.* **57,** 147-155
11. Ip, C., Dong, Y., and Ganther, H. E. (2002) *Cancer Metastasis Rev.* **21,** 281-289
12. Ursini, F., Heim, S., Kiess, M., Maiorino, M., Roveri, A., Wissing, J., and Flohe, L. (1999) *Science* **285,** 1393-1396
13. Martin-Romero, F. J., Kryukov, G. V., Lobanov, A. V., Carlson, B. A., Lee, B. J., Gladyshev, V. N., and Hatfield, D. L. (2001) *J. Biol. Chem.* **276,** 29798-29804
14. Su, D., Novoselov, S. V., Sun, Q. A., Moustafa, M. E., Zhou, Y., Oko, R., Hatfield, D. L., and Gladyshev, V. N. (2005) *J. Biol. Chem.* **280,** 26491-26498
15. Gladyshev, V. N., Jeang, K. T., Wootton, J. C., and Hatfield, D. L. (1998) *J. Biol. Chem.* **273,** 8910-8915
16. Korotkov, K. V., Novoselov, S. V., Hatfield, D. L., and Gladyshev, V. N. (2002) *Mol. Cell. Biol.* **22,** 1402-1411
17. Delaglio, F., Grzesiek, S., Vuister, G. W., Zhu, G., Pfeifer, J., and Bax, A. (1995) *J. Biomol. NMR* **6,** 277-293
18. Johnson, B. A. (2004) *Methods Mol. Biol.* **278,** 313-352
19. Neri, D., Szyperski, T., Otting, G., Senn, H., and Wuthrich, K. (1989) *Biochemistry* **28,** 7510-7516
20. Chou, J. J., Gaemers, S., Howder, B., Louis, J. M., and Bax, A. (2001) *J. Biomol. NMR* **21,** 377-382
21. Cornilescu, G., Delaglio, F., and Bax, A. (1999) *J. Biomol. NMR* **13,** 289-302
22. Habeck, M., Rieping, W., Linge, J. P., and Nilges, M. (2004) *Methods Mol. Biol.* **278,** 379-402
23. Koradi, R., Billeter, M., and Wuthrich, K. (1996) *J. Mol. Graph.* **14,** 51-55
24. Zweckstetter, M., and Bax, A. (2000) *J. Am. Chem. Soc.* **122,** 3791-3792
25. Su, D., and Gladyshev, V. N. (2004) *Biochemistry* **43,** 12177-12188
26. Aslund, F., Berndt, K. D., and Holmgren, A. (1997) *J. Biol. Chem.* **272,** 30780-30786
27. Holm, L., and Park, J. (2000) *Bioinformatics* **16,** 566-567
28. Holm, L., and Sander, C. (1998) *Nucleic Acids Res.* **26,** 316-319
29. Brockmann, C., Diehl, A., Rehbein, K., Strauss, H., Schmieder, P., Korn, B., Kuhne, R., and Oschkinat, H. (2004) *Structure (Camb)* **12,** 1645-1654
30. Saarinen, M., Gleason, F. K., and Eklund, H. (1995) *Structure* **3,** 1097-1108
31. Weichsel, A., Gasdaska, J. R., Powis, G., and Montfort, W. R. (1996) *Structure* **4,** 735-751
32. Martin, J. L. (1995) *Structure* **3,** 245-250
33. Qi, Y., and Grishin, N. V. (2005) *Proteins* **58,** 376-388
34. Dyson, H. J., Jeng, M. F., Tennant, L. L., Slaby, I., Lindell, M., Cui, D. S., Kuprin, S., and Holmgren, A. (1997) *Biochemistry* **36,** 2622-2636
35. Lappi, A. K., Lensink, M. F., Alanen, H. I., Salo, K. E., Lobell, M., Juffer, A. H., and Ruddock, L. W. (2004) *J. Mol. Biol.* **335,** 283-295
36. Holmgren, A. (1995) *Structure* **3,** 239-243
37. Lundstrom, J., and Holmgren, A. (1993) *Biochemistry* **32,** 6649-6655
38. Mossner, E., Huber-Wunderlich, M., and Glockshuber, R. (1998) *Protein Sci.* **7,** 1233-1244
39. Inaba, K., and Ito, K. (2002) *EMBO J.* **21,** 2646-2654
40. Huber-Wunderlich, M., and Glockshuber, R. (1998) *Fold. Des.* **3,** 161-171
41. Behne, D., Hilmert, H., Scheid, S., Gessner, H., and Elger, W. (1988) *Biochim. Biophys. Acta* **966,** 12-21
42. Hill, K. E., Lyons, P. R., and Burk, R. F. (1992) *Biochem. Biophys. Res. Commun.* **185,** 260-263
43. Alanen, H. I., Williamson, R. A., Howard, M. J., Lappi, A. K., Jantti, H. P., Rautio, S. M., Kellokumpu, S., and Ruddock, L. W. (2003) *J. Biol. Chem.* **278,** 28912-28920
44. Anelli, T., Alessio, M., Mezghrani, A., Simmen, T., Talamo, F., Bachi, A., and Sitia, R. (2002) *EMBO J.* **21,** 835-844
45. Kemmink, J., Darby, N. J., Dijkstra, K., Nilges, M., and Creighton, T. E. (1996) *Biochemistry* **35,** 7684-7691
46. Labunskyy, V. M., Ferguson, A. D., Fomenko, D. E., Chelliah, Y., Hatfield, D. L., and Gladyshev, V. N. (2005) *J. Biol. Chem.* **280,** 37839-37845
47. Korotkov, K. V., Kumaraswamy, E., Zhou, Y., Hatfield, D. L., and Gladyshev, V. N. (2001) *J. Biol. Chem.* **276,** 15330-15336
48. Pollock, S., Kozlov, G., Pelletier, M. F., Trempe, J. F., Jansen, G., Sitnikov, D., Bergeron, J. J., Gehring, K., Ekiel, I., and Thomas, D. Y. (2004) *EMBO J.* **23,** 1020-1029 Frickel, E. M., Riek, R., Jelesarov, I., Helenius, A., Wuthrich, K., and Ellgaard, L. (2002) *Proc. Natl. Acad. Sci. U. S. A.* **99,** 1954-1959
50. Zapun, A., Darby, N. J., Tessier, D. C., Michalak, M., Bergeron, J. J., and Thomas, D. Y. (1998) *J. Biol. Chem.* **273,** 6009-6012
51. Meunier, L., Usherwood, Y. K., Chung, K. T., and Hendershot, L. M. (2002) *Mol. Biol. Cell* **13,** 4456-4469
52. DeLano, W. (2002) *The PyMOL Molecular Graphic System*, DeLano Scientific, San Carlos, CA
53. Poirot, O., Suhre, K., Abergel, C., O'Toole, E., and Notredame, C. (2004) *Nucleic Acids Res.* **32** (Web Server issue), 37-40
54. Farmer, B. T., 2nd, Constantine, K. L., Goldfarb, V., Friedrichs, M. S., Wittekind, M., Yanchunas, J., Jr., Robertson, J. G., and Mueller, L. (1996) *Nat. Struct. Biol.* **3,** 995-997
55. Laskowski, R. A., Rullmannn, J. A., MacArthur, M. W., Kaptein, R., and Thornton, J. M. (1996) *J. Biomol. NMR* **8,** 477-486

SUPPLEMENTAL TABLE ONE. **DALI comparisons using the structure of the redox domain of SelM that is closest to the mean of the ensemble**

PDB	Z-score	Sequence Identity	Protein
2a4h	9.9	22%	Fruit fly Sep15
1s3a	7.4	14%	Subunit B8 from human NADH ubiquinone oxidoreductase complex I
1thx	5.4	12%	*Anabaena* thioredoxin 2
1b9y	4.9	6%	Bull transducin βγ fragment
1erv	4.7	10%	Human thioredoxin mutant
1a8y	4.7	5%	Rabbit calsequestrin

SUPPLEMENTAL TABLE TWO. **DALI comparisons using the structure of the redox domain of Sep15 that is closest to the mean of the ensemble**

PDB	Z-score	Sequence Identity	Protein
2a2p	9.9	22%	Mouse SelM
1s3a	6.1	16%	Subunit B8 from human NADH ubiquinone oxidoreductase complex I
1erv	4.8	11%	Human thioredoxin mutant
1xvw	4.6	8%	*Mycobacterium tuberculosis* AhpE
1thx	4.2	10%	*Anabaena* thioredoxin 2
1a8y	4.2	9%	Rabbit calsequestrin

SUPPLEMENTAL FIGURE 1. **Stereoviews of structural comparisons.** *A*, Backbone superposition of SelM (magenta) and Sep15 (yellow). *B*, Backbone superposition of SelM (magenta) and human thioredoxin (yellow).